Cell. Mol. Life Sci. (2015) 72:869–883
DOI 10.1007/s00018-014-1826-6

Cellular and Molecular Life Sciences

MULTI-AUTHOR REVIEW

Electron transfer and reaction mechanism of laccases

Stephen M. Jones · Edward I. Solomon

Received: 23 December 2014 / Accepted: 30 December 2014 / Published online: 9 January 2015

Abstract Laccases are part of the family of multicopper oxidases (MCOs), which couple the oxidation of substrates to the four electron reduction of O_2 to H_2O. MCOs contain a minimum of four Cu's divided into Type 1 (T1), Type 2 (T2), and binuclear Type 3 (T3) Cu sites that are distinguished based on unique spectroscopic features. Substrate oxidation occurs near the T1, and electrons are transferred approximately 13 Å through the protein via the Cys-His pathway to the T2/T3 trinuclear copper cluster (TNC), where dioxygen reduction occurs. This review outlines the electron transfer (ET) process in laccases, and the mechanism of O_2 reduction as elucidated through spectroscopic, kinetic, and computational data. Marcus theory is used to describe the relevant factors which impact ET rates including the driving force, reorganization energy, and electronic coupling matrix element. Then, the mechanism of O_2 reaction is detailed with particular focus on the intermediates formed during the two $2e^-$ reduction steps. The first $2e^-$ step forms the peroxide intermediate, followed by the second $2e^-$ step to form the native intermediate, which has been shown to be the catalytically relevant fully oxidized form of the enzyme.

Keywords Laccase · Multicopper oxidase · Type 1 copper · Type 2 copper · Type 3 copper · Marcus theory

S. M. Jones · E. I. Solomon (✉)
Department of Chemistry, Stanford University, 333 Campus Drive, Stanford, CA 94305, USA
e-mail: solomone@stanford.edu

Introduction

Laccases belong to a family of enzymes known as multicopper oxidases (MCOs), which oxidize a variety of substrates while performing the four electron reduction of dioxygen to water [1–4]. MCOs can be divided into two broad categories: those with high substrate specificity, and those with low substrate specificity. The first category contains the metalloxidases such as Fet3p [5, 6] and ceruloplasmin (Cp) [6, 7], which selectively oxidize iron in yeast and mammals, respectively. Ascorbate oxidase [8] and laccases [1–3] are examples of the latter category, which oxidize a range of organic molecules to facilitate processes such as lignin formation [9] or degradation [10], and wound healing in plants [11]. Laccases are common in fungi including in the polypore mushroom *Trametes versicolor*, and the white-rot fungus *Pleurotus ostreatus* [12], and well known in a number of plants, in particular the lacquer tree *Rhus vernicifera* [13–16]. The first bacterial laccase was reported in the rhizospheric bacterium *Azospirillum lipoferum* [17], and several others have since been characterized [18, 19]. The most widely studied of these prokaryotic laccases is the CotA laccase from *Bacillus subtilis*, now technically classified as a bilirubin oxidase (BOD) [20].

Structurally, MCOs contain at least four copper atoms, which can be classified into three types based on their unique spectroscopic features. In the oxidized state, the Type 1 copper (T1) exhibits an intense ($\varepsilon \sim 5{,}000\ M^{-1}\ cm^{-1}$) absorption feature at ~600 nm due to a $S(Cys)_\pi \rightarrow Cu(II)$ charge transfer (CT) transition, and a small parallel hyperfine coupling constant in EPR ($A_{\|} = 40\text{–}90 \times 10^{-4}\ cm^{-1}$), both resulting from the highly covalent nature of the Cu–S(Cys) bond [21]. The Type 2 (T2) Cu(II) shows no significant absorbance feature, but has a parallel hyperfine coupling

constant similar to that of a typical tetragonal copper center ($A_{\|} = 140–200 \times 10^{-4}$ cm^{-1}) [22, 23]. Binuclear Type 3 (T3) copper sites are EPR silent due to antiferromagnetic (AF) coupling resulting from a bridging hydroxo ligand between the coppers in the resting oxidized state. This hydroxo bridge is also responsible for the intense absorbance at 330 nm assigned to μ_2-OH → T3Cu(II) CT transitions [24]. Figure 1 shows the UV–Vis absorbance and EPR spectra of the resting oxidized (RO) state in the MCOs as described above.

Based on known crystal structures and sequence alignment, the ligation of the four copper centers is largely conserved among MCOs. The T1 site is coordinated by a minimum of two His and one Cys residues [25, 26]. In many MCOs, a fourth ligand, Met, binds axially, resulting in a four coordinate (4C) trigonally elongated tetrahedral geometry as shown in Fig. 2a. This Cu–S(Met) bond is substantially longer and weaker than the other three ligand bonds to the T1 [27]. This structure appears in the redox active T1 sites in Cp, and in plant laccases. Alternatively, Fig. 2b shows the three coordinate (3C) trigonal planar structure present in fungal laccases and Fet3p, which results when a non-coordinating, hydrophobic residue, such as Phe or Leu, is present in the protein in place of the axial Met. The effects of these perturbations are discussed in Part

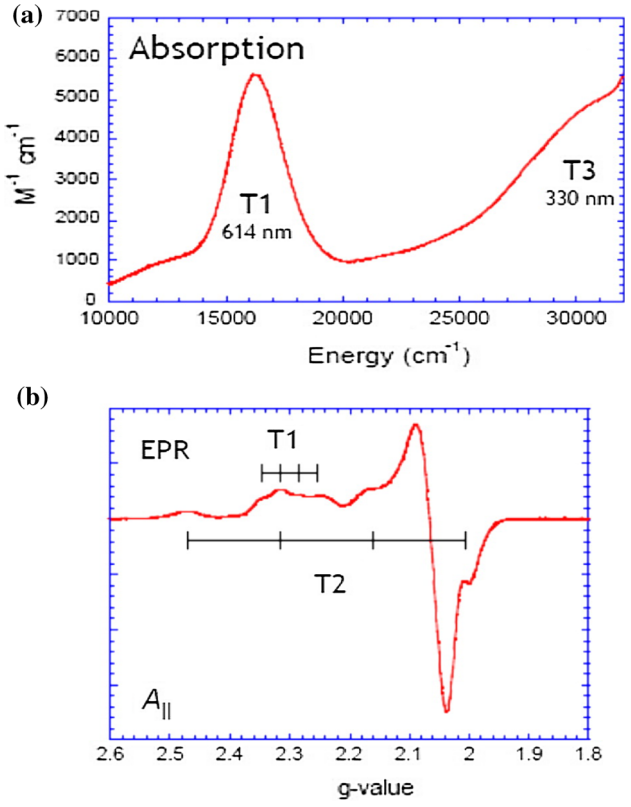

Fig. 1 UV-Vis absorbance (**a**) and EPR spectra (**b**) of resting laccase. Reprinted with permission from [3]. Copyright 2014 American Chemical Society

II. The T2 and binuclear T3 copper sites are arranged in a trinuclear copper cluster (TNC) approximately 13 Å distant from the T1 Cu. Type 1 sites are connected to the two T3 coppers of the TNC via a conserved His-Cys-His triad. Figure 3 shows the crystal structure of the TNC from *T. versicolor* laccase (*Tv*L). Including the two His ligands from the Cys-His bridge, there are a total of eight His residues coordinated to the TNC coppers. The T3 Cu's each have three His ligands, and in the oxidized state, a bridging μ_2-OH ligand resulting in approximately trigonal bipyramidal geometry with an open equatorial coordination position directed into the TNC. The T2 Cu(II) is ligated to two His and one hydroxo ligand (external to the cluster) in a square planar geometry, also with an open coordination position directed into the TNC [28].

Additionally, there are two conserved second-sphere carboxylate residues located close to the TNC. One carboxylate is situated on the side of the TNC closest to the T2-T3β edge. Mutational studies have shown that this moiety is required for catalytic activity [29]. Another conserved carboxylate is situated below the T3 site. This residue has been shown to play a key role in the protonation of oxygen-derived products of catalysis [30], described below.

The focus of this review is on understanding inter- and intramolecular electron transfer (ET) properties of laccases, and outlining the mechanism of O_2 reaction. The first section deals with electron transfer from the substrate to the T1 Cu, and then from the T1 site to the TNC. The next section describes the mechanism of O_2 reduction through the known spectroscopic intermediates, and describes the role of the native intermediate (NI) in catalysis.

Electron transfer properties of the T1 copper

Type 1, or "blue copper," sites are well known in bioinorganic chemistry for their ET properties [21, 27, 31, 32]. In MCOs, substrate oxidation occurs at the T1, which then rapidly transfers electrons through the Cys-His pathway to the TNC [33, 34]. The first- and second-sphere residues surrounding the T1 control both the intermolecular ET to the T1 from the substrate, and the intramolecular ET from the T1 to the TNC.

Semi-classical Marcus theory provides the description of ET in metalloenzymes. The electron transfer rate constant, k_{ET}, is given by the following equation [35]

$$k_{ET} = K_A S \sqrt{\frac{4\pi^3}{h^2 \lambda k_B T}} |H_{DA}|^2 \exp\left(\frac{-(\Delta G^\circ + \lambda)^2}{4\lambda k_B T}\right), \quad (1)$$

where K_A is the equilibrium constant for the electron donor–acceptor complex, S is a steric term to account for

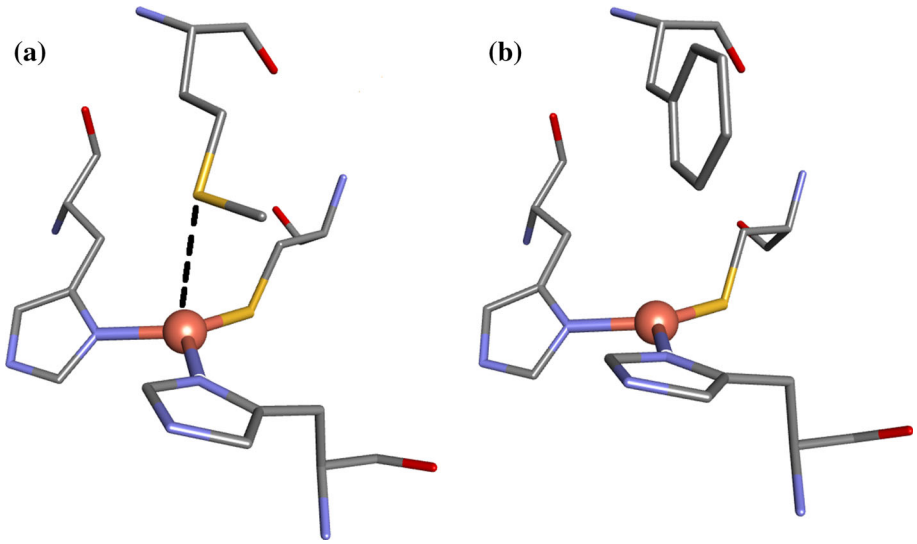

Fig. 2 T1 sites of CotA from *B. subtilis* with axial methionine (**a**) and of laccase from *T. versicolor* without the axial methionine (**b**). PDB accession numbers: 2X88 and 1GYC

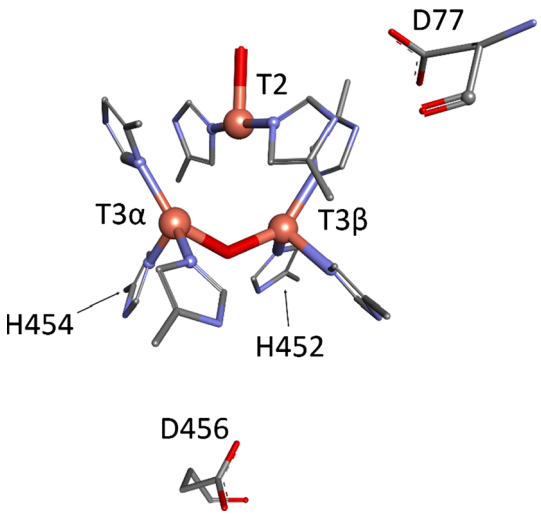

Fig. 3 T2 and T3 Cu sites in MCOs. Labeled histidines H454 and H452 connect T3α and T3β to the T1 Cu through the Cys-His bridge. Also shown are conserved carboxylates D77 and D456. All residues are numbered according to PDB:1GYC

asymmetry in complex formation conducive to ET, λ is the reorganization energy, H_{DA} is the electronic coupling matrix element between the donor and acceptor, and $\Delta G°$ is the free energy difference for electron transfer. For intermolecular ET from substrate to T1, the most obvious parameters that influence k_{ET} are the reorganization energy, λ, and the electronic driving force, $\Delta G°$.

The reorganization energy is the energy required for ligand and solvent rearrangements between initial and final states during ET. These inner- and outer-sphere contributions combine to give the total reorganization energy ($\lambda_i + \lambda_o = \lambda_{total}$) [35]. Inner-sphere reorganization energies are associated with changes in the first coordination sphere of the metal atom, and outer-sphere reorganization energies account for changes in the rest of the protein and solvent rearrangements [36]. Crystallography and X-ray absorption fine structure (EXAFS) data show only minimal differences between oxidized and reduced structures of T1 sites in most MCOs. The changes seen upon oxidation are primarily shortening ligand-Cu bonds, with very little angular change. Significantly, the Jahn–Teller tetragonal distortion associated with oxidation of most copper complexes is not observed in blue copper sites. This is a result of the ligands and the geometry at the T1, which split the Cu $3d_{x^2-y^2}$ and $3d_{xy}$ levels, eliminating the degeneracy required for electron-nuclear coupling that would result in this geometric distortion [27]. These data indicate that λ_i is small for ET in blue copper sites, and indeed, inner-sphere reorganization energies are calculated to be on the order of 0.5 eV [37, 38]. For comparison, the inner-sphere reorganization energy of a representative copper tetrammine complex is ~1.4 eV [37]. There may, however, be considerable contributions to the total reorganization energies from the substrate (when the T1 accepts the electron), or from the TNC (when the T1 donates the electron). These contributions to λ_{total} would then contribute to k_{ET} through Eq. 1. Changes in reorganization energies which arise from the structural differences of reactive intermediates are found to make relatively minor contributions to the changes in ET rates seen during the catalytic cycle of MCOs (vide infra). We turn now to the free energy difference, $\Delta G°$, which derives from the reduction potentials of T1 Cu sites.

Reduction potentials ($E°$) of blue copper sites in laccases range from ~400 to ~800 mV versus NHE [13, 39–41]. Although many factors influence reduction potentials of metal sites in proteins [42], one significant contribution in MCOs is the presence or absence of an axial Met ligand.

Plant laccases, which possess the Met ligand, often have potentials on the low end of this range, while fungal laccases, which lack an axial ligand, typically have higher reduction potentials [43]. Evidence for the impact of axial ligation on $E°$ can be seen in two mutants of CotA in *B. subtilis*. Wild type (WT) CotA has a reduction potential of 455 mV, but when the T1 axial ligand Met502 is replaced with non-ligating Phe (M502F) or Leu (M502L), the potentials of these mutants increase to 548 and 515 mV, respectively [44]. Conversely, mutation of the axially non-coordinating F463 residue to Met in *T. villosa* laccase (*Tvi*L) decreases the reduction potential from 790 to 680 mV [45]. Clearly, the presence of the additional Cu–S(Met) bond decreases the reduction potential of the T1 Cu, yet $E°$ can differ substantially even among blue copper proteins with identical ligand sets.

Comparisons of T1 centers over a range of copper proteins have revealed that the strength of the Cu–S(Met) bond can profoundly impact the electronic and geometric structures of these sites. Decreasing the Cu–S(Met) bond length results in weakening and lengthening of the Cu–S(Cys) bond, accompanied by a tetragonal (i.e., Jahn–Teller) distortion of the site, in which the Cu–S(Cys)-S(Met) plane rotates into the Cu–N(His)-N(His) plane [46]. This "coupled distortion" describes the continuum of geometries connecting blue copper sites to the so-called green copper sites that possess the same 1Cys-2His-1Met ligand motif seen in plant laccases, but differ in electronic and geometric structure. The extremes of this coupled distortion coordinate are the green T1 site in *Achromobacter cycloclastes* nitrite reductase (NiR), which has a strong Cu–S(Met) bond, and the blue T1 Cu in plant laccases and plastocyanin, which have weak Cu–S(Met) bonds (and, by extension, T1 sites in fungal laccases and Fet3p, in which no axial ligand is present) [21, 27]. Effects of this perturbation are manifested in spectroscopic changes including the S(Cys) $\rightarrow$ Cu π and σ CT bands switching from intense π/weak σ in blue sites to intense σ/weak π in green sites. Density functional theory (DFT) calculations calibrated to spectroscopic data and spectroscopy on NiR variants indicate that it is the strength of the Cu–S(Met) bond that determines whether a site is blue (weak) or green [strong Cu–S(Met) bond] [47]. This, in turn, is a result of the protein backbone, which constrains the Cu–S(Met) bond and enforces an active site structure at a given point along the coupled distortion coordinate. A protein constraint on active site ligation to enhance function is often referred to as the entatic, or rack state [48]. The axial Met constraint contributes to tuning the reduction potential of the T1 as described below.

A demonstration of the importance of the protein backbone comes from the T1 site in *Rhodobacter sphaeroides* NiR, in which the flexible nature of the methionine-containing loop allows the axial Met bond to the T1 to break at high temperatures. Breaking the Cu–S(Met) bond is entropically favored, and this results in a thermodynamic equilibrium between green sites (bound Met) that predominate at low temperature and blue sites (unbound Met) that are present at higher temperatures. Temperature-dependent spectroscopic data in conjunction with DFT calculations yielded Cu–S(Met) bond enthalpies (ΔH) of 4.6 and $\sim$1 kcal/mol for the oxidized and reduced sites, respectively. Thus, the presence of the Cu–S(Met) bond stabilizes the oxidized state relative to the reduced state [49]. Most T1 sites do not have flexibility in the protein backbone and do not readily interconvert from blue to green sites [50]. Keeping the ligand bound (i.e., opposing entropy) provides a mechanism (i.e., an "entatic state") by which the Cu–S(Met) distance enforced by the protein structure stabilizes the oxidized relative to the reduced state to tune down the reduction potential of the T1 by several hundred millivolts.

It is important to emphasize here that the effect of the axial ligand alone is not sufficient to explain the range of reduction potentials exhibited across T1 Cu sites. Other factors that contribute to $E°$ differences among T1 Cu centers include the hydrophobicity of nearby residues, hydrogen bonding to the S(Cys), and electrostatic interactions in the protein backbone [51, 52]. The effects on $E°$ due to hydrogen bonds and protein dipole interactions have been investigated [53, 54]. Mutations of second-sphere residues surrounding the T1 center in *Pseudomonas aeruginosa* azurin resulted in significant changes in reduction potential. These variants included removal of the hydrogen bond to the S(Cys), as well as deletion or insertion of carbonyl dipoles near the Cu–S(Cys) bond. Two types of contributions to tuning $E°$ were identified as follows: covalent contributions, which change the covalency of the Cu–S(Cys) bond, and non-local electrostatic contributions, which serve only to change the relative energies of the electrons in the redox active molecular orbital (RAMO). Various spectroscopies and in-silico experiments were used to quantify each contribution to the potential. Overall, covalent contributions were found to account for a $\sim$10 mV decrease in $E°$ for each percent increase in sulfur character of the RAMO. These covalent effects either added to or opposed electrostatic contributions, which consisted mainly of electron-dipole interactions [54]. This study provides insight into how second-sphere residues near the T1 Cu also play an important role in tuning the reduction potential over several hundred millivolts.

We now consider the first two terms in the Marcus equation, K_A and S, which describe the interactions between substrate and the protein in the vicinity of the T1 Cu. Increasing K_A or S through favorable binding between substrate and enzyme, and at the proper position for ET,

increases the electron transfer rate. This requires an understanding of substrate binding in MCOs.

Phenols and amines are the natural substrates of laccases [55], although some also oxidize inorganic ions [56–58]. The broad range of organic substrates capable of being oxidized by laccases is a result of non-covalent binding near the T1 His ligands for outer-sphere ET. A solved crystal structure by Bertrand and coworkers [59] included the substrate 2,5-xylidine hydrogen-bonded to *Tv*L through the carboxylate D206 and the Nε2 of H458, a first sphere ligand to the T1 Cu. Although the orientation of the substrate can differ, comparisons to other amino acid sequences and crystal structures show that this solvent exposed His binding site is common in laccases [60–63]. Kinetic studies on several laccases yielded Michaelis constants (K_m) which varied by substrate, but were similar across the enzymes studied, suggesting similar substrate-binding sites for these enzymes. Data also show that in laccases an outer-sphere ET to the T1 is the rate-determining step in turnover [40, 64, 65]. This is in contrast to metalloxidases, such as Fet3p, which have smaller K_m values due to favorable Fe(II)-binding sites at the carboxylate residues E185 and D409 [66, 67]. These carboxylates are then hydrogen-bonded to the His residues of the T1 site, providing an efficient ET pathway in these metalloxidases. Single and double mutations of each of these residues to Ala change the coordination environment at the substrate, decreasing the effectiveness of Fet3p as a metalloxidase and turning on laccase-like activity [68, 69]. Another interesting result of these mutational studies involves the E185D mutant of Fet3p. This mutant exhibits the same T1 reduction potential as the WT enzyme and the same K_m, yet the electron transfer rate is an order of magnitude slower than the WT. This is attributed to changes in the hydrogen-bonding network that disrupts the ET pathway [68]. This leads us to the next term in the Marcus equation: H_{DA}.

The electronic coupling matrix element, H_{DA}, is primarily dependent on three factors: (1) the covalency of the ligand–metal bond, (2) the anisotropy of the redox active molecular orbital, and (3) the orbital overlap of the superexchange pathway between donor and acceptor through the protein [27]. For ET from the substrate to the T1 in MCOs, the short distance between donor and acceptor leads to minimal attenuation of the electronic coupling and therefore a relatively large H_{DA}. As noted above, the E185D mutant of Fet3p shows that disrupting the superexchange pathway from the substrate to the T1 greatly decreases H_{DA} [68]. In laccases, the through bond pathway from substrate to the T1 is shorter since the binding occurs near a nitrogen of the histidine ligated directly to the T1, suggesting a reasonable electronic coupling constant despite the limited covalency of the Cu–N(His) bond. The T1 site is well positioned, however, to rapidly transfer electrons to the TNC due to the highly covalent Cu–S(Cys) bond.

In laccases, the covalency and anisotropy in the ground state, as well as the Cys-His superexchange pathway contribute to a large H_{DA} for intramolecular ET from the T1 to the TNC. The RAMO, a Cu $d_{x^2-y^2}$ orbital, contains a substantial contribution from the S(Cys) p_π orbital [70–72]. UV-visible absorption (UV-Vis), X-ray absorption (XAS), circular dichroism (CD), and magnetic CD (MCD) spectroscopies explicitly quantify the ground state wavefunction of the oxidized T1 site. This lowest unoccupied beta molecular orbital (β-LUMO) is shown in Fig. 4a. Through Cu L-edge and S K-edge XAS, it has been determined that the RAMO of blue copper sites contains ~42 % Cu character, and ~38 % S character [73]. Compared to $CuCl_4^{2-}$, a "normal" Cu complex with 61 % Cu character in the ground state [74], this represents a substantial increase in covalency of the T1 Cu. Simultaneous fitting of the UV-Vis, and MCD spectra reveal a strong S(Cys)p_π → Cu(II) ligand to metal charge transfer (LMCT) transition and weak S(Cys)p_σ → Cu(II) LMCT [71]. This relationship is the inverse of normal copper and green copper sites which have a strong p_σ LMCT and a weak p_π LMCT (vide supra). These data show that in blue copper sites, the Cu–S(Cys) bond bisects the Cu $d_{x^2-y^2}$ orbital of the copper, resulting in considerable overlap with the S p_π orbital. This highly covalent π-anisotropy of the Cu–S(Cys) bond in the ground state of the oxidized Cu activates the site for rapid intramolecular ET through the Cys-His pathway to the TNC.

The Cys-His pathway provides a link through the protein backbone between the Cu–S(Cys) π bond at the T1 to the Cu–N(His) σ bond at the T3 site [21, 27, 75, 76]. There is an additional hydrogen-bond overlap, shown in Fig. 4b, c, which serves as an additional superexchange pathway that also contributes to H_{DA} in MCOs [75]. Numerous studies have shown a strong interaction between the T1 and TNC. Augustine and coworkers, working with Fet3p, studied the effects of mutating the His ligands at the T3 Cu sites to Cys and Gln. Resonance Raman (rR) spectroscopy revealed that this weakened the bonds at the T3 Cu and strengthened the T1 Cu–S(Cys) bond. A decreased reduction potential of the T1 sites in these mutants was attributed to this increased donation of the S p_π orbital to the Cu [77]. Changes in Cu–S(Cys) bonding were proposed to arise due to a conformational change of the pathway, which would result in changes to H_{DA}.

A recent computational study by Hadt, et al. [75] on the Cys-His pathway in NiRs and MCOs quantifies how the anisotropy (π versus σ overlap) and covalency (% S contribution) of the T1 Cu–S(Cys) bond significantly changes H_{DA}. Models of the Cys-His pathway in NiRs and MCOs were used to probe the differences between blue and green

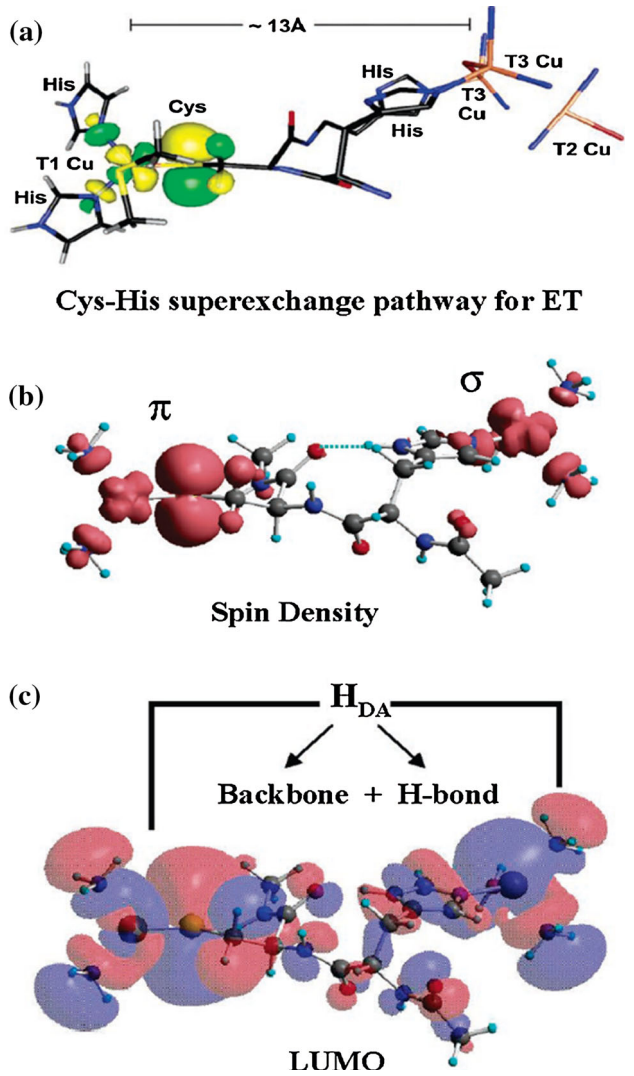

Fig. 4 β-LUMO coupled into Cys-His pathway (**a**). Calculated spin density of ground state wavefunction with H-bond pathway shown in *blue* (**b**). π to σ superexchange pathway from T1 Cu to TNC (**c**). Reprinted with permission from [21]. Copyright 2006 American Chemical Society

T1 sites. This study showed a direct correlation between the covalency of the Cu–S(Cys) bond (% S character) and H_{DA} and that k_{ET} goes as $(H_{DA})^2$ in non-adiabatic ET (Eq. 1). Blue and green sites were also found to activate different superexchange pathways in the same bridge, which led to marked changes in H_{DA}. In MCOs, the hydrogen-bond pathway in Fig. 4b, in addition to the Cys-His π to σ pathway, results in large H_{DA}'s from the blue T1 sites. If, instead, a green site existed in MCOs, H_{DA}'s would be small. Conversely, in NiRs, structural differences in this same H-bond pathway result in larger H_{DA}'s for green relative to blue T1 sites [75]. It is worth noting that additional, unstudied pathways exist in MCOs between the T1 and the other Cu's in the TNC that may lead to additional constructive or destructive interferences for ET. However, it is clear that the highly covalent, π-donor bonding, blue copper site in laccases promotes rapid intramolecular ET during the catalytic cycle.

The above discussion of electron transfer processes described by Marcus theory as applied to blue copper sites illustrates how rates of electron transfer depend sensitively on several terms, and changes in the first and second-sphere ligand environment can result in significant changes to the relevant terms in the ET rate expression. Laccases are highly tuned by nature to accept electrons from substrates, and shuttle them to the TNC, where dioxygen is reduced. In one of the most widely studied MCOs, *Rv*L, intramolecular ET must be fast given a maximal turnover rate of 560 s^{-1} [15], and kinetic data show that during turnover this electron transfer rate has a lower limit of 700 s^{-1} [78]; however, pulse radiolysis studies on the resting enzyme give a rate of 1.1 s^{-1} [79]. This indicates that k_{ET} changes during the course of the catalytic cycle, and suggests that it is dependent on the state of the TNC. In fact, the resting site as described by crystallography is not the catalytically relevant fully oxidized form of the TNC. This will be discussed in the following section, which explores the mechanism of O_2 reduction through the known spectroscopic intermediates.

O_2 reduction mechanism

The mechanism of O_2 reduction by MCOs has been determined through a large body of spectroscopic, kinetic, and computational studies of native enzymes, and mutated or otherwise chemically altered derivatives. Investigations have largely focused on the two most widely studied MCOs, *Rv*L and Fet3p, where selective perturbations of the different copper sites stabilize certain reactive intermediates which can then be characterized spectroscopically. Figure 5 shows an overview of the mechanism, which begins with the fully reduced enzyme, followed by two $2e^-$ steps that reduce O_2 to H_2O. The catalytic cycle then continues with the re-reduction of the fully oxidized intermediate formed upon reduction of dioxygen rather than reduction of the resting enzyme (vide infra).

The resting oxidized (RO) form of the enzyme (Fig. 5, bottom left) has four oxidized coppers including a hydroxide-bridged T3 center with the spectroscopic features described above and shown in Fig. 1. The mechanism begins when a suitable reductant donates four electrons to reduce all four Cu(II) atoms to Cu(I). Electrons enter through the T1 and are transferred to the TNC. In the absence of a redox active T1 site, no reduction of the TNC is observed upon addition of native substrates. However, in these altered enzymes, the T2 and T3 sites can still be

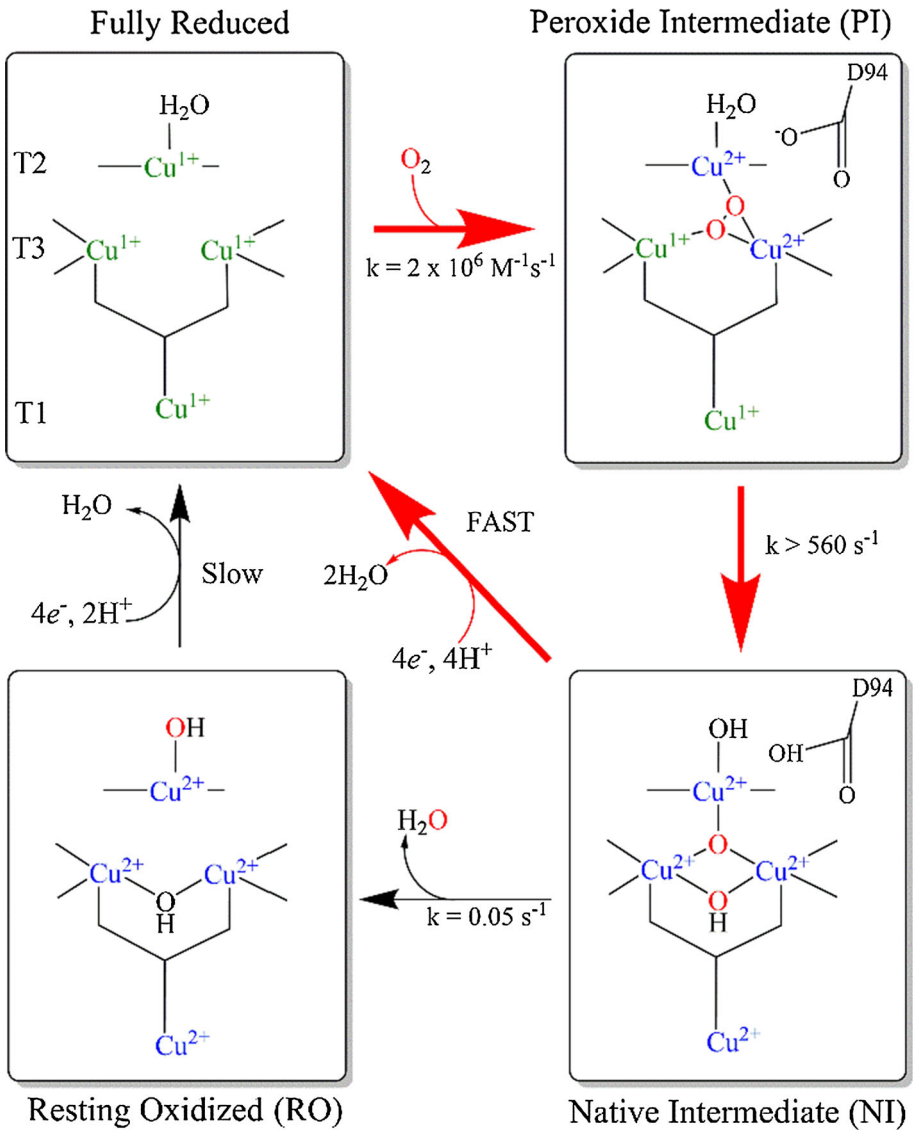

Fig. 5 Mechanism of O_2 reduction by MCOs. *Red arrows* show steps in the catalytic cycle. *Black arrows* show reduction of resting enzyme to enter catalytic cycle and decay of the native intermediate which terminates catalysis. Adapted with permission from [80]. Copyright 2010 American Chemical Society

reduced with smaller, inner-sphere reductants, and the reduced TNC, even in the absence of the T1, will react with and reduce O_2. Elimination of T1 reactivity was accomplished either through site-selective mutation which inhibits Cu loading at the T1, resulting in a T1 depleted enzyme (T1D) [81], or through a derivative of tree laccase in which the T1 Cu has been replaced by the redox innocent Hg^{2+} ion (T1Hg) [82, 83]. These derivatives have been crucial to the elucidation of the mechanism of O_2 reduction at the TNC, as described below.

Anaerobic reduction of resting laccases reveals complex, pH-dependent reduction behavior for the four copper sites. There remains some ambiguity in the exact steps involved in Cu(II) reduction, but it is clear that formation of a fully reduced TNC is required for O_2 reaction (vide infra). The Cu(II) sites are essentially fully reduced after addition of ~4 electron equivalents, although the order in which each site becomes reduced varies among enzymes and reaction conditions [13, 84–87]. The binuclear T3 Cu site reduces as a two electron acceptor, which is supported by the lack of a half-met [i.e., Cu(II)Cu(I)] T3 EPR signal during reduction of the resting enzyme. The T2 is often the last site to fully reduce during anaerobic titrations [13]; however, where clear data exist, all 4 Cu(II)s reduce at approximately the same potential.

In T1D/T1Hg, the fully reduced TNC reacts with dioxygen to form the peroxide intermediate (PI) with a bimolecular rate constant of $\sim 2 \times 10^6\ M^{-1}\ s^{-1}$ [88, 89]. In the absorbance spectrum of PI, there are two CT bands at 340 and 480 nm (Fig. 6). These two CT bands decompose into four bands in CD. Also present in CD are several ligand field (d → d) transitions signaling the presence of oxidized copper [88]; yet PI lacks of any paramagnetic features in either EPR or MCD, indicating an S = 0 ground

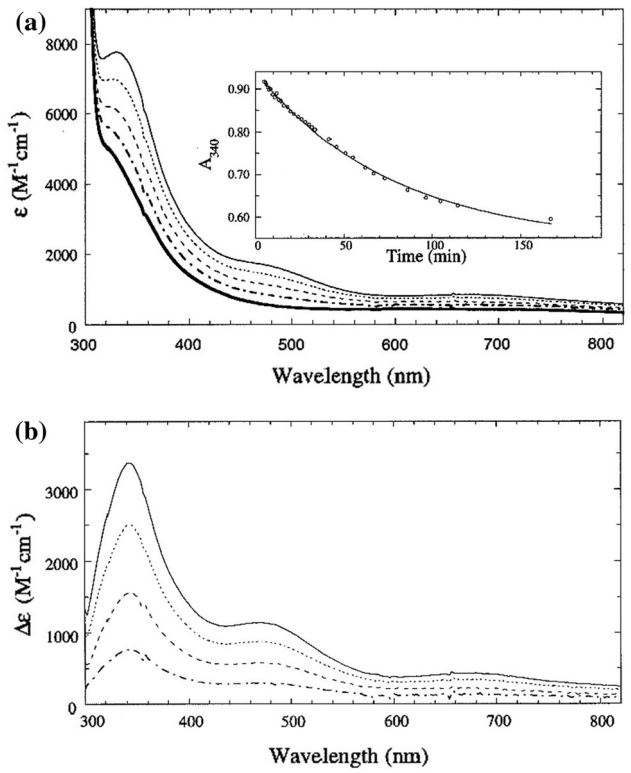

Fig. 6 **a** Absorbance spectra of the peroxy intermediate at different times during its decay. *Inset* shows the decay at 340 nm. **b** Absorbance difference spectra of the spectra in (**a**) relative to fully oxidized T1Hg laccase. Reprinted with permission from [90]. Copyright 1996 American Chemical Society

state. Furthermore, SQUID magnetic susceptibility studies confirm that it is diamagnetic with strong AF coupling between two Cu(II)s ($-2\ J > 200\ cm^{-1}$). Isotope ratio mass spectrometry (IRMS) with $^{18}O_2$ showed that PI retains both oxygen atoms from the reaction with O_2 [90]. It decays slowly to a species with an MCD spectrum identical to the features of the native intermediate (NI, vide infra), and subsequently to a species with an EPR spectrum of an oxidized T2 Cu as in the resting form [19]. PI is therefore a catalytically competent precursor to the NI, which is discussed below. These findings lead to the assignment of PI as a peroxide-level species, with peroxide bridging two oxidized coppers of the TNC, leaving one reduced.

Although they were originally considered the same, it is important to note the distinction between the binuclear T3 center in the TNC and the binuclear Cu sites found in the coupled binuclear Cu proteins hemocyanin (Hc) or tyrosinase (Tyr). In Hc and Tyr, reduced copper sites reversibly bind O_2 to form a planar μ-η^2:η^2 peroxo-bridged structure (oxy Hc) [91], similar to the hypothetical T3 site shown in Fig. 7a. Although both PI and oxy Hc exhibit antiferromagnetic coupling of two Cu(II)s, their distinct CT spectra reveal a large geometric difference between these two peroxide-bound species [92]. Moreover, when the T2 Cu of *Rv*L is selectively eliminated (T2D), the reduced T3 site is unreactive toward O_2 [92]. This reduced T3 site is still capable of binding small molecules, but in contrast to Hc and Tyr, exogenous ligands do not bridge the T3 Cu centers. The origin of these differences lies in the protein architecture around the active sites. In reduced Hc (deoxy Hc), the Cu(I)–Cu(I) distance is tightly constrained by the protein to ~4.2 Å, which destabilizes deoxy Hc and activates it for O_2 binding. Reduced T3 sites in laccases are more flexible with equilibrium Cu–Cu distances of ~6.5 Å, leading to less electrostatic repulsion and a more stable reduced site, which explains its lack of O_2 reactivity [93]. These data show that not only is the T3 site in laccases different from the binuclear site in Hc, but also that the presence of the T2 Cu is required for O_2 reaction in laccases leading to PI formation.

Mutational studies provide further insight into the structure of the TNC of PI. T1D mutants of Fet3p, expressed with either the T3α or T3β Cu sites (see Fig. 3 for labels) selectively deactivated due to a His to Gln T3 ligand mutation, showed that the T2 and T3β coppers are electron donors in the first $2e^-$ step of O_2 reduction [80]. Other mutational studies involved transformation of the conserved carboxylate D94 (D77 in Fig. 3) in Fet3p. Enzymes with D94 transformed to Ala or Asn were unreactive toward O_2, yet the D94E mutant still formed PI upon reaction with O_2, showing that an anionic residue at this position was required for reactivity [29]. Computational models that include the negative charge arising from this residue yielded the μ_3-1,1,2 peroxo bridging structure shown in Fig. 7b [94]. Electronic structure calculations of PI indicate that the negative charge of D94 lowers the reduction potential of the T2 and T3β sites, allowing them

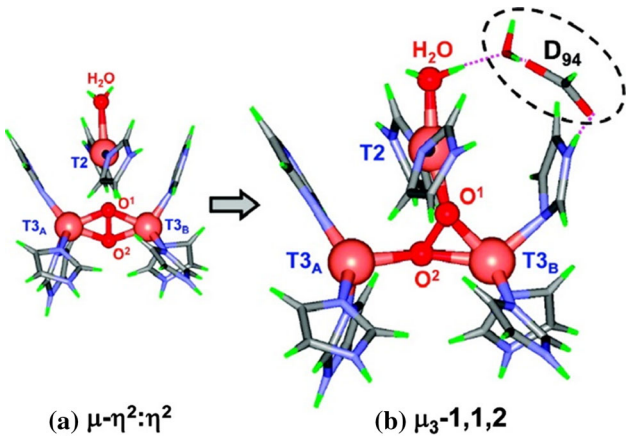

Fig. 7 Optimized structures of the peroxy intermediate without (**a**) and with (**b**) the D94 residue. Reprinted with permission from [94]. Copyright 2007 American Chemical Society

to donate the two electrons to O_2. This results in a peroxide-bridged site that has good overlap of the O_2^{2-} π_σ* HOMO with the $d_{x^2-y^2}$ LUMOs on the T2 and T3β Cu(II)s, consistent with the strong AF coupling observed in PI [94]. Thus, in contrast to the coupled binuclear Cu sites in Hc and Tyr, the TNC is set up to bind O_2 as peroxide bridging all three Cu centers. This geometry is essential for the reductive cleavage of the O–O bond.

The next step in the mechanism is the decay of PI through O–O bond cleavage. In the absence of T1 Cu, PI decay exhibits an $^{18}O_2$ kinetic isotope effect (KIE) of 1.11 indicating that O–O cleavage is part of the rate-limiting step [95]. Furthermore, at low pH, the rate is modestly enhanced, and exhibits an inverse solvent kinetic isotope effect (SKIE) of 0.89 in Fet3p. Increasing the pH slows the decay rate and eliminates the SKIE. In Fet3p, when E487, the carboxylate nearer the T3 Cu site (D456 in Fig. 3), is mutated to Ala, the pH effect is eliminated. The E487D mutant still exhibits a rate increase at low pH, but shows a "normal" SKIE of 2.0. Meanwhile, mutation of D94, the carboxylate at the T2/T3β edge, to Glu changes the SKIE to 2.3 [30]. All three mutations result in slower PI decay rates, indicating that these carboxylates are critical for proton transfers during the reductive cleavage of peroxide. Similar findings were later reported in T1D CotA, in which mutations of E498 (equivalent to D456 in Fig. 3) to Leu, and D116 (D77 in Fig. 3) to Ala each slowed PI formation and essentially halted PI decay. Similarly, the T1D-E498D and T1D-D116E CotA mutants formed PI at similar rates to WT, but exhibited significantly slower PI decay rates [96, 97]. The model which explains these observations involves two O–O cleavage reaction pathways: a proton-unassisted pathway at high pH and a proton-assisted pathway at low pH as shown in Fig. 8 [30, 94]. Both pathways invoke proton donation to peroxide from E487 through the H-bond network to an oxygen atom bridging the T3 Cu's. This model also includes the effect of the D94 residue, which is responsible for deprotonating the water bound to the reduced T2 upon its oxidation. The resulting hydroxide lowers the reduction potential of the T2, facilitating electron transfer to the peroxide. Computation of the potential energy surface for PI decay in the holo enzyme begins with an additional electron, which would be donated from the T1 Cu(I), to form a PI + e^- species. At low pH, the proton is transferred first from E487 to the oxygen bridging the T3 [O^2 in Fig. 7(b)], followed by reductive cleavage of the O–O bond. In accordance with the Westheimer model, the inverse SKIE is attributed to a product-like transition state in which the stronger O–H bond of the μ_2-OH has formed and the weaker carboxylate O–H proton donor bond is broken. At high pH, peroxide O–O bond elongation occurs first, followed by proton transfer after the transition state [30]. The activation energy for the former, proton-assisted pathway is slightly lower compared to the proton-unassisted pathway, which is consistent with the limited rate increase at low pH. Both activation energies are also in line with the experimental activation energy of ~3–5 kcal/mol [94].

Figure 9 shows the 2-D potential energy surface calculated for this conversion of PI to NI. Examining the orbital contributions to the RAMOs during the reaction pathway shows that the TNC is set up for this reaction with good orbital overlap between the e^- donating HOMOs on the T2 and T3α Cu's (both reduced) and the LUMO, the O_2^{2-} σ* orbital. The T3β is already oxidized in forming PI, but in the triangular topology of the TNC contributes to the reaction by acting as a Lewis acid in lowering the energy of the peroxide σ* electron acceptor orbital [94]. A schematic of this interaction is shown in Fig. 10. This overlap allows for cleavage of the O–O bond with the concerted, two-electron reduction of peroxide, a highly exothermic process.

The formation of NI from PI (Fig. 5, bottom right) must be rapid in holo laccases with reported second-order NI formation rate constants of 0.7–5 $\mu M^{-1}s^{-1}$ [88, 98]. From Cu K-edge XAS, all four coppers are oxidized in NI, with characteristic absorbance features at 318, 330, 365, and 614 nm. NI exhibits an $S = 1/2$ ground state determined through MCD with EPR g values of 2.15, 1.86, and 1.65 in low temperature (<20 K) EPR [99]. Importantly, it has a low lying excited state at ~150 cm^{-1} observed in temperature-dependent MCD and in the temperature-dependent saturation behavior of the low g value EPR signals [100]. NI must therefore have an all bridged trinuclear Cu(II) cluster. EXAFS shows a Cu–Cu distance of 3.3 Å, which, through magneto-structural correlations, gives an isotropic exchange coupling (−2 J) of 520 cm^{-1} from one pair of Cu(II)s. Inclusion of two more bridging interactions closing the 3 Cu(II) triangle results in a condition known as spin frustration in which all three spins want to be, but cannot be AF coupled. This results in the low lying excited state at 150 cm^{-1}, which restricts the range of possible values for the three exchange coupling constants. These isotropic coupling constants for the other two bridges were determined by evaluating the contribution from each Cu(II) to the ground and excited state C terms in MCD. The resulting analysis yields exchange coupling constants (−2 J) of 430 and 470 cm^{-1} for the other two bridges [100]. This spin frustration also gives rise to the g values below 2.0 due to a phenomenon known as antisymmetric exchange [101]. This requires good ground state to ground state exchange coupling between two adjacent Cu(II)s, spin orbit coupling between the ground and excited states on a single Cu(II), and exchange coupling between this excited state and the ground state on the adjacent Cu(II). The result is that in the EPR experiment,

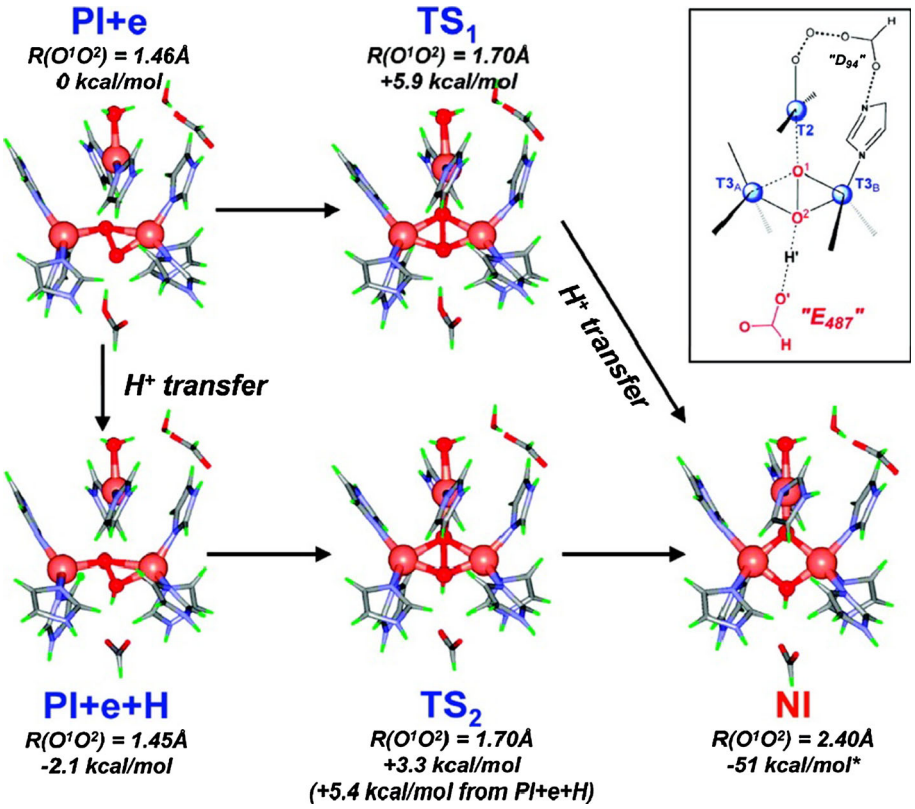

Fig. 8 Schematic showing the roles of carboxylates E487 and D94 in O–O bond cleavage during PI decay. Reprinted with permission from [94]. Copyright 2007 American Chemical Society

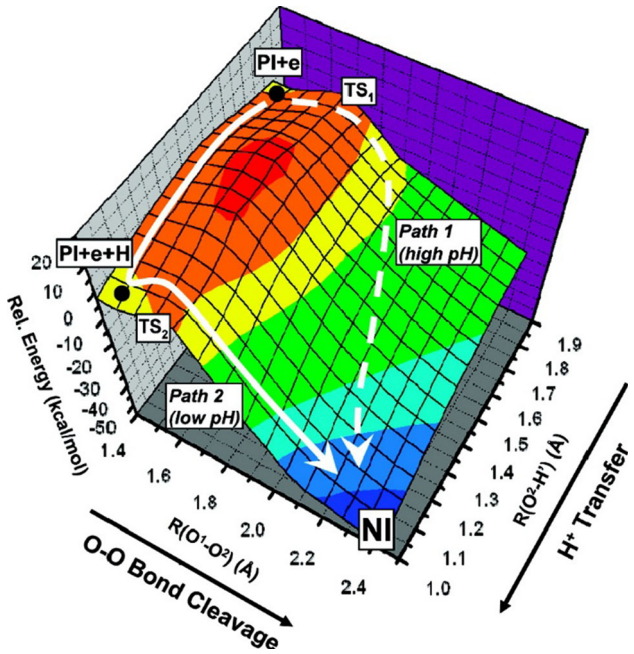

Fig. 9 2D potential energy surface of the decay of the peroxy intermediate. Reprinted with permission from [94]. Copyright 2007 American Chemical Society

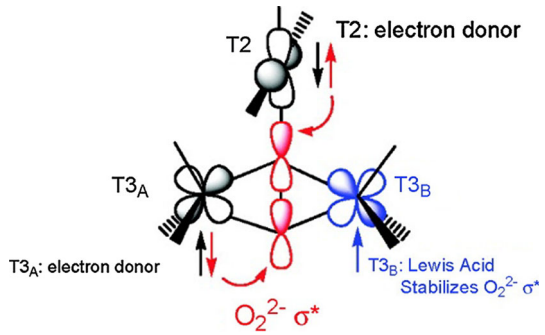

Fig. 10 Schematic of the overlap between the HOMOs on the T2 and T3α sites and the O_2^{2-} σ* orbital. Reprinted with permission from [94]. Copyright 2007 American Chemical Society

for fields perpendicular to the 3 Cu(II) plane, there is a non-linear, field dependent mixing of the ground and a low lying excited state that gives rise to $g_\perp \ll 2$, as shown in Fig. 11 (right). Finally, analysis of the orbital contributions to the pseudo-A terms in MCD (i.e., two C terms with opposite signs) based on studies of structurally defined relevant model complexes identified the structure of NI as a μ_3-oxo bridged species with a μ_2-OH bridge between the T3 Cu(II)s as shown in Fig. 12 [102]. Further protonation of the μ_2-hydroxide bridge has not occurred as this would result in a ferromagnetic ground state, which is not observed experimentally [103]. Both oxygen atoms come from O–O cleavage, and the μ_2-OH remains bound.

Although both NI and RO have fully oxidized TNCs, they exhibit very different spectral properties and

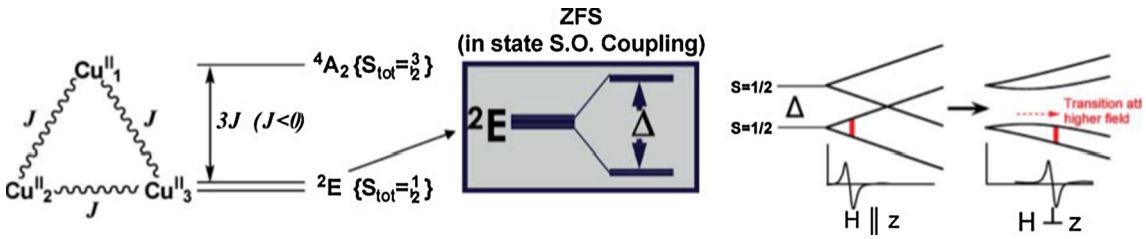

Fig. 11 Origin of the low g values observed in NI. Reprinted from [104] with permission of The Royal Society of Chemistry

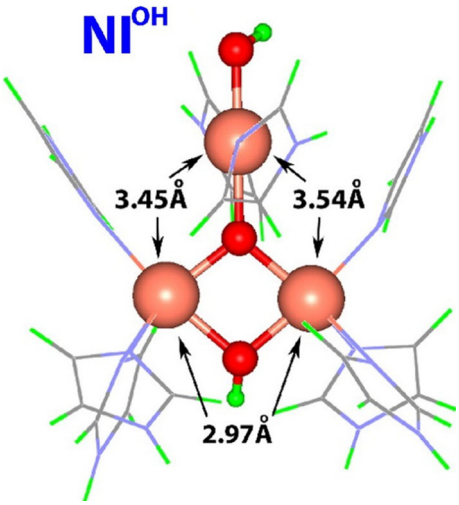

Fig. 12 Optimized structure of the NI. Reprinted from [103]. Copyright 2007 National Academy of Science, USA

reactivities due to their different oxygen bridges (μ_3-O and μ_2-OH in NI and μ_2-OH in RO). In the absence of excess reductant, NI decays slowly to the RO form with an observed rate constant of $\sim$0.05 s^{-1} [78, 105]. IRMS on $^{18}O_2$ revealed that one of the oxygen atoms from dioxygen remained bound to the TNC in RO [90, 106]. A model linking the NI structure to RO requires the addition of protons and the loss of H_2O. Protonation of the μ_3-oxo bridge is energetically favorable relative to protonation at the μ_2-hydroxo ligand, and the protonated μ_3-oxo rotates through the T2-T3α edge with a calculated barrier of 8.5 kcal/mol, which is consistent with the experimentally observed barrier of 8.8–13.9 kcal/mol in the decay of NI to the resting enzyme [103]. Importantly, the rate of decay of NI is several orders of magnitude slower than catalytic turnover, which is further evidence that RO is not part of the catalytic cycle. Instead, as summarized below, NI has been shown to be the fully oxidized form of the enzyme that is relevant to catalysis.

It has been observed that the turnover rate of *Rv*L (560 s^{-1}) was significantly higher than either the T1–T3 electron transfer rates in RO (1.1 s^{-1}), or the decay of NI to RO (0.05 s^{-1}). For this reason, the RO form of the enzyme is not catalytically relevant. Instead, re-reduction of NI has now been shown to be the catalytically relevant reduction step. The kinetics of RO reduction versus re-reduction of NI were studied via stopped flow absorption spectroscopy [78]. The two processes show markedly different behaviors for the T1 and T3 electron transfer rates. In RO, the T1 reduces quickly, followed by slow reduction of the T3 at an initial rate of 0.111 s^{-1} at 4 °C. In contrast, the rate of T1 to T3 ET in the first e^- reduction of NI was observed to be $>$700 s^{-1}. Both processes are proton-coupled electron transfers (PCET), and this dramatic change in k_{ET} between the two fully oxidized TNC's is due to the substantially higher basicity of the μ_3-oxo ligand of NI relative to the μ_2-OH ligand present in the RO structure [78]. The increased proton affinity of the μ_3-oxo species drives the PCET enabling fast re-reduction of NI.

DFT calculations were used to evaluate changes in the parameters of the ET rate equation. The differences in driving force between these two PCET steps reveal that NI reduction is 7 kcal/mol more favorable than reduction of RO. In these calculations, the reorganization energy for the first PCET in NI reduction is $\sim$0.3 eV lower than for reduction of RO. Using these values in the Marcus equation (with H_{DA} held constant) yield a factor of 10^3 greater ET rate for NI reduction, in agreement with experimental data [78]. The structure of NI is therefore responsible for rapid turnover, since reductive cleavage of the O–O bond forms the μ_3-oxo ligand and allows for proton coupling leading to fast re-reduction and high turnover rates.

The mechanism described here likely applies in general to all MCOs. Turnover rates of laccases vary widely among substrates, but are generally several orders of magnitude greater than rates measured for metalloxidases [6, 15, 98]. Although PI has not been observed in native enzymes, it has been observed in several MCOs lacking a T1 center, including derivatives of *Rv*L [107], Fet3p [89], CueO [108], and CotA [97]. PI forms at a rate consistent with it being in the reduction of O_2. NI-like features have been observed in *Rv*L, BOD [109], Cp [105, 110], and CueO [108]. Interestingly, in some MCOs including BOD, Cp, and CueO, NI features are not long lived; however, in both CueO and BOD, mutations at sites equivalent to E487 in

Fet3p result in more pronounced NI features [108, 111]. This suggests that although differences in second-sphere residues around the Cu centers may lead to changes in rates for individual mechanistic steps, the intermediates described here are common to all MCOs. Future studies will expand this model to include other relevant features that exert a mechanistic influence on different MCO activities.

Conclusion

In laccases, the enzyme ET properties, largely governed by the T1 Cu, combined with the unique triangular topology of the TNC effectively couple the oxidation of substrates to the reduction of dioxygen. As illustrated above, structural constraints imposed by the protein modulate electron and proton transfer rates both to and from the T1 Cu, and at the site of O_2 reduction. Reductive cleavage of the O–O bond, effectively a $4e^-$ process, leads to the formation of a species, NI, that is then poised for rapid proton-coupled reduction to generate H_2O and continue the catalytic cycle.

It is fascinating to consider that while laccases and other MCOs have nearly identical Cu active sites they exhibit substantial diversity in substrate interactions and catalytic rates. As structure–function relationships are established for second-sphere residues that explain differences in reactivity, it will be interesting to correlate these changes to the roles that particular enzymes serve in biological systems. Understanding how enzyme activity is regulated by changes in electron and/or proton transfer rates will both provide fundamental insight into how nature controls the fundamentally important process of O_2 reduction to H_2O and also be important to the development of industrial processes and biomedical applications.

Acknowledgments SMJ would like to thank Drs. Dave Heppner and Christian Kjaergaard for their contributions to this study and for many illuminating conversations on MCOs. EIS is indebted to all his past students and collaborators upon whose science this review is based. This research is supported by NIH Grant R01DK031450. The content is solely the responsibility of the authors and does not necessarily represent the official views of the National Institutes of Health.

References

1. Solomon EI, Sundaram UM, Machonkin TE (1996) Multicopper oxidases and oxygenases. Chem Rev 96:2563–2606
2. Giardina P, Faraco V, Pezzella C et al (2010) Laccases: a never-ending story. Cell Mol Life Sci 67:369–385. doi:10.1007/s00018-009-0169-1
3. Solomon EI, Heppner DE, Johnston EM et al (2014) Copper active sites in biology. Chem Rev 114:3659–3853. doi:10.1021/cr400327t
4. Messerschmidt A (1997) Multi-copper oxidases. World Scientific, River Edge
5. Shi X, Stoj C, Romeo A et al (2003) Fre1p Cu2+ reduction and Fet3p Cu1+ oxidation modulate copper toxicity in Saccharomyces cerevisiae. J Biol Chem 278:50309–50315. doi:10.1074/jbc.M307019200
6. Stoj C, Kosman DJ (2003) Cuprous oxidase activity of yeast Fet3p and human ceruloplasmin: implication for function. FEBS Lett 554:422–426. doi:10.1016/S0014-5793(03)01218-3
7. Hellman NE, Gitlin JD (2002) Ceruloplasmin metabolism and function. Annu Rev Nutr 22:439–458. doi:10.1146/annurev.nutr.22.012502.114457
8. Messerschmidt A (1998) Metal sites in small blue copper proteins, blue copper oxidases and vanadium-containing enzymes. Struct Bond 90:37–68
9. O'Malley DM, Whetten R, Bao W et al (1993) The role of laccase in lignification. Plant J 4:751–757
10. Leonowicz A, Cho N-S, Luterek J et al (2001) Fungal laccase: properties and activity on lignin. J Basic Microbiol 41:185–227
11. Mayer AM, Staples RC (2002) Laccase : new functions for an old enzyme. Phytochemistry 60:551–565. doi:10.1016/S0031-9422(02)00171-1
12. Baldrian P (2006) Fungal laccases–occurrence and properties. FEMS Microbiol Rev 30:215–242. doi:10.1111/j.1574-4976.2005.00010.x
13. Reinhammar BRM, Vanngard TI (1971) The electron-accepting sites in rhus vernicifera laccase as studied by anaerobic oxidation-reduction titrations. Eur J Biochem 18:463–468
14. Dooley DM, Rawlings J, Dawson JH et al (1979) Spectroscopic studies of rhus vernicifera and polyporus versicolor laccase. electronic structures of the copper sites. J Am Chem Soc 101:5038–5046
15. Petersen LCHR, Degn H (1978) Steady-state kinetics of laccase from rhus vernicifera. Biochim Biophys Acta 526:85–92
16. Johnson DL, Thompson JL, Brinkmann SM et al (2003) Electrochemical characterization of purified Rhus vernicifera laccase: voltammetric evidence for a sequential four-electron transfer. Biochemistry 42:10229–10237. doi:10.1021/bi034268p
17. Givaudan A, Effosse A, Faure D et al (1993) Polyphenol oxidase in Azospirillum lipoferum isolated from rice rhizosphere: evidence for laccase activity in non-motile strains of Azospirillum lipoferum. FEMS Microbiol Lett 108:205–210
18. Sharma P, Goel R, Capalash N (2006) Bacterial laccases. World J Microbiol Biotechnol 23:823–832. doi:10.1007/s11274-006-9305-3
19. Zoppellaro G, Sakurai T, Huang H (2001) A novel mixed valence form of Rhus vernicifera laccase and its reaction with dioxygen to give a peroxide intermediate bound to the trinuclear center. J Biochem 129:949–953
20. Durand F, Kjaergaard CH, Suraniti E et al (2012) Bilirubin oxidase from Bacillus pumilus: a promising enzyme for the elaboration of efficient cathodes in biofuel cells. Biosens Bioelectron 35:140–146. doi:10.1016/j.bios.2012.02.033
21. Solomon EI (2006) Spectroscopic methods in bioinorganic chemistry: blue to green to red copper sites. Inorg Chem 45:8012–8025. doi:10.1021/ic060450d
22. Malmström BG, Reinhammar B, Vänngård T (1968) Two forms of copper (II) in fungal laccase. Biochim Biophys Acta 156:67–76. doi:10.1016/0304-4165(68)90105-0
23. Malmström BG, Reinhammar B, Vänngård T et al (1970) The state of copper in stellacyanin and laccase from the lacquer tree Rhus vernicifera. Biochim Biophys Acta 205:48–57. doi:10.1016/0005-2728(70)90060-5
24. Cole JL, Clark PA, Solomon EI (1990) Spectroscopic and chemical studies of the laccase trinuclear copper active site: geometric and electronic structure. J Am Chem Soc 112:9534–9548
25. Gray HB, Malmström BG, Williams RJP (2000) Copper coordination in blue proteins. J Biol Inorg Chem 5:551–559. doi:10.1007/s007750000146

26. Sakurai T, Kataoka K (2007) Structure and function of type I copper in multicopper oxidases. Cell Mol Life Sci 64:2642–2656. doi:10.1007/s00018-007-7183-y
27. Solomon EI, Szilagyi RK, DeBeer George S, Basumallick L (2004) Electronic structures of metal sites in proteins and models: contributions to function in blue copper proteins. Chem Rev 104:419–458. doi:10.1021/cr0206317
28. Quintanar L, Yoon J, Aznar CP et al (2005) Spectroscopic and electronic structure studies of the trinuclear Cu cluster active site of the multicopper oxidase laccase : nature of its coordination unsaturation. J Am Chem Soc 127:13832–13845
29. Quintanar L, Stoj C, Wang T-P et al (2005) Role of aspartate 94 in the decay of the peroxide intermediate in the multicopper oxidase Fet3p. Biochemistry 44:6081–6091. doi:10.1021/bi047379c
30. Augustine AJ, Quintanar L, Stoj CS et al (2007) Spectroscopic and kinetic studies of perturbed trinuclear copper clusters: the role of protons in reductive cleavage of the O–O bond in the multicopper oxidase Fet3p. J Am Chem Soc 129:13118–13126. doi:10.1021/ja073905m
31. Sykes AG (1991) Active-site properties of the blue copper proteins. Adv Inorg Chem 36
32. Canters GW, Gilardi G (1993) Engineering type 1 copper sites in proteins. FEBS Lett 325:39–48. doi:10.1016/0014-5793(93)81410-2
33. Solomon E, Lowery MD (1993) Electronic structure contributions to function in bioinorganic chemistry. Science 259:1575–1581
34. Wherland S, Farver O, Pecht I (2014) Multicopper oxidases: intramolecular electron transfer and O_2 reduction. J Biol Inorg Chem 19:541–554. doi:10.1007/s00775-013-1080-7
35. Marcus RA, Sutin N (1985) Electron transfers in chemistry and biology. Biochim Biophys Acta 811:265–322
36. Warren JJ, Lancaster KM, Richards JH, Gray HB (2012) Inner- and outer-sphere metal coordination in blue copper proteins. J Inorg Biochem 115:119–126. doi:10.1016/j.jinorgbio.2012.05.002
37. Olsson MH, Ryde U, Roos BO (1998) Quantum chemical calculations of the reorganization energy of blue-copper proteins. Protein Sci 7:2659–2668. doi:10.1002/pro.5560071220
38. Ryde U, Olsson MHM (2001) Structure, strain, and reorganization energy of blue copper models in the protein. Int J Quantum Chem 81:335–347
39. Xu F, Berka RM, Wahleithner JA et al (1998) Site-directed mutations in fungal laccase: effect on redox potential, activity and pH profile. Biochem J 334:63–70
40. Xu F (1997) Effects of redox potential and hydroxide inhibition on the pH activity profile of fungal laccases. J Biol Chem 272:924–928. doi:10.1074/jbc.272.2.924
41. Schneider P, Caspersen MB, Mondorf K et al (1999) Characterization of a *Coprinus cinereus* laccase. Enzym Microb Technol 25:502–508. doi:10.1016/S0141-0229(99)00085-X
42. Li H, Webb SP, Ivanic J, Jensen JH (2004) Determinants of the relative reduction potentials of type-1 copper sites in proteins. J Am Chem Soc 126:8010–8019. doi:10.1021/ja049345y
43. Battistuzzi G, Bellei M, Leonardi A et al (2005) Reduction thermodynamics of the T1 Cu site in plant and fungal laccases. J Biol Inorg Chem 10:867–873. doi:10.1007/s00775-005-0035-z
44. Durão P, Bento I, Fernandes AT et al (2006) Perturbations of the T1 copper site in the CotA laccase from Bacillus subtilis: structural, biochemical, enzymatic and stability studies. J Biol Inorg Chem 11:514–526. doi:10.1007/s00775-006-0102-0
45. Xu F, Palmer AE, Yaver DS et al (1999) Targeted mutations in a trametes villosa laccase : axial perturbations of the T1 copper. J Biol Chem 274:12372–12375
46. Lacroix LB, Randall DW, Nersissian AM et al (1998) Spectroscopic and geometric variations in perturbed blue copper centers : electronic structures of stellacyanin and cucumber basic protein. J Am Chem Soc 120:9621–9631
47. Basumallick L, Szilagyi RK, Zhao Y et al (2003) Spectroscopic studies of the met182thr mutant of nitrite reductase : role of the axial ligand in the geometric and electronic structure of blue and green copper sites. J Am Chem Soc 125:14784–14792
48. Vallee BL, Williams RJP (1967) Metalloenzymes: the entatic nature of their active sites. Proc Natl Acad Sci USA 59:498–505
49. Ghosh S, Xie X, Dey A et al (2009) Thermodynamic equilibrium between blue and green copper sites and the role of the protein in controlling function. Proc Natl Acad Sci USA 106:4969–4974. doi:10.1073/pnas.0900995106
50. Xie X, Hadt RG, Pauleta SR et al (2009) A variable temperature spectroscopic study on Paracoccus pantotrophus pseudoazurin: protein constraints on the blue Cu site. J Inorg Biochem 103:1307–1313. doi:10.1016/j.jinorgbio.2009.04.012
51. Marshall NM, Garner DK, Wilson TD et al (2009) Rationally tuning the reduction potential of a single cupredoxin beyond the natural range. Nature 462:113–116. doi:10.1038/nature08551
52. Berry SM, Baker MH, Reardon NJ (2010) Reduction potential variations in azurin through secondary coordination sphere phenylalanine incorporations. J Inorg Biochem 104:1071–1078. doi:10.1016/j.jinorgbio.2010.06.004
53. Hong G, Ivnitski DM, Johnson GR et al (2011) Design parameters for tuning the type 1 Cu multicopper oxidase redox potential: insight from a combination of first principles and empirical molecular dynamics simulations. J Am Chem Soc 133:4802–4809. doi:10.1021/ja105586q
54. Hadt RG, Sun N, Marshall NM et al (2012) Spectroscopic and DFT studies of second-sphere variants of the type 1 copper site in azurin: covalent and nonlocal electrostatic contributions to reduction potentials. J Am Chem Soc 134:16701–16716. doi:10.1021/ja306438n
55. Reiss R, Ihssen J, Richter M et al (2013) Laccase versus laccase-like multi-copper oxidase: a comparative study of similar enzymes with diverse substrate spectra. PLoS ONE 8:e65633. doi:10.1371/journal.pone.0065633
56. Hofer C, Schlosser D (1999) Novel enzymatic oxidation of Mn2+‡ to Mn 3+‡ catalyzed by a fungal laccase. FEBS Lett 451:186–190
57. Gorbacheva M, Morozova O, Shumakovich G et al (2009) Enzymatic oxidation of manganese ions catalysed by laccase. Bioorg Chem 37:1–5. doi:10.1016/j.bioorg.2008.09.002
58. Ricklefs E, Winkler N, Koschorreck K, Urlacher VB (2014) Expanding the laccase-toolbox: a laccase from Corynebacterium glutamicum with phenol coupling and cuprous oxidase activity. J Biotechnol. doi:10.1016/j.jbiotec.2014.05.031
59. Bertrand T, Jolivalt C, Briozzo P et al (2002) Crystal structure of a four-copper laccase complexed with an arylamine: insights into substrate recognition and correlation with kinetics. Biochemistry 41:7325–7333
60. Enguita FJ, Marçal D, Martins LO et al (2004) Substrate and dioxygen binding to the endospore coat laccase from Bacillus subtilis. J Biol Chem 279:23472–23476. doi:10.1074/jbc.M314000200
61. Matera I, Gullotto A, Tilli S et al (2008) Crystal structure of the blue multicopper oxidase from the white-rot fungus Trametes trogii complexed with p-toluate. Inorganica Chim Acta 361:4129–4137. doi:10.1016/j.ica.2008.03.091
62. Polyakov KM, Fedorova TV, Stepanova EV et al (2009) Structure of native laccase from Trametes hirsuta at 1.8 a resolution. Acta Crystallogr D Biol Crystallogr 65:611–617. doi:10.1107/S0907444909011950

63. Hakulinen N, Kiiskinen L-L, Kruus K et al (2002) Crystal structure of a laccase from Melanocarpus albomyces with an intact trinuclear copper site. Nat Struct Biol 9:601–605. doi:10.1038/nsb823
64. Xu F (1996) Oxidation of phenols, anilines, and benzenethiols by fungal laccases: correlation between activity and redox potentials as well as halide inhibition. Biochemistry 35:7608–7614. doi:10.1021/bi952971a
65. Xu F, Shin W, Brown SH et al (1996) A study of a series of recombinant fungal laccases and bilirubin oxidase that exhibit significant differences in redox potential, substrate specificity, and stability. Biochim Biophys Acta 1292:303–311
66. Quintanar L, Gebhard M, Wang T-P et al (2004) Ferrous binding to the multicopper oxidases Saccharomyces cerevisiae Fet3p and human ceruloplasmin: contributions to ferroxidase activity. J Am Chem Soc 126:6579–6589. doi:10.1021/ja049220t
67. Taylor AB, Stoj CS, Ziegler L et al (2005) The copper-iron connection in biology: structure of the metallo-oxidase Fet3p. Proc Natl Acad Sci USA 102:15459–15464. doi:10.1073/pnas.0506227102
68. Stoj CS, Augustine AJ, Zeigler L et al (2006) Structural basis of the ferrous iron specificity of the yeast ferroxidase, Fet3p. Biochemistry 45:12741–12749. doi:10.1021/bi061543+
69. Kosman DJ (2008) Substrate entasis and electronic coupling elements in electron transfer from Fe in a multicopper ferroxidase. Inorganica Chim Acta 361:844–849. doi:10.1016/j.ica.2007.10.013
70. Penfield KW, Gewirth AA, Solomon EI (1985) Electronic structure and bonding of the blue copper site in plastocyanin. J Am Chem Soc 107:4519–4529. doi:10.1021/ja00301a024
71. Gewirth AA, Solomon EI (1988) Electronic structure of plastocyanin: excited state spectral features. J Am Chem Soc 110:3811–3819
72. Solomon EI, Penfield KW, Gewirth AA et al (1996) Electronic structure of the oxidized and reduced blue copper sites: contributions to the electron transfer pathway, reduction potential, and geometry. Inorganica Chim Acta 243:67–78
73. George SJ, Lowery MD, Solomon EI, Cramer SP (1993) Copper L-edge spectral studies: a direct experimental probe of the ground-state covalency in the blue copper site in plastocyanin. J Am Chem Soc 115:2968–2969
74. Gewirth AA, Cohen SL, Schugar HJ, Solomon EI (1987) Spectroscopic and theoretical studies of the unusual epr parameters of distorted tetrahedral cupric sites: correlations to x-ray spectral features of core levels. Inorg Chem 26:1133–1146
75. Hadt RG, Gorelsky SI, Solomon EI (2014) Anisotropic covalency contributions to superexchange pathways in type one copper active sites. J Am Chem Soc. doi:10.1021/ja508361h
76. Farver O, Pecht I (1991) Long range electron transfer in blue copper proteins. Mol Cryst Liq Cryst 194:215–224. doi:10.1080/00268949108041167
77. Augustine AJ, Kragh ME, Sarangi R et al (2008) Spectroscopic studies of perturbed t1 cu sites in the multicopper oxidases saccharomyces cerevisiae Fet3p and Rhus vernicifera laccase : allosteric coupling between the T1 and trinuclear Cu sites. Biochemistry 47:2036–2045
78. Heppner DE, Kjaergaard CH, Solomon EI (2013) Molecular origin of rapid versus slow intramolecular electron. J Am Chem Soc 135:12212–12215
79. Farver O, Wherland S, Koroleva O et al (2011) Intramolecular electron transfer in laccases. FEBS J 278:3463–3471. doi:10.1111/j.1742-4658.2011.08268.x
80. Augustine AJ, Kjaergaard C, Qayyum M et al (2010) Systematic perturbation of the trinuclear copper cluster in the multicopper oxidases: the role of active site asymmetry in its reduction of O2 to H2O. J Am Chem Soc 132:6057–6067. doi:10.1021/ja909143d
81. Blackburn NJ, Ralle M, Hassett R, Kosman DJ (2000) Spectroscopic analysis of the trinuclear cluster in the Fet3 protein from yeast, a multinuclear copper oxidase. Biochemistry 39:2316–2324
82. Morie-bebel MM, Morris MC, Menzie JL, McMillin DR (1984) A mixed-metal derivative of laccase containing Mercury(II) in the Type 1 binding site. J Am Chem Soc 106:3677–3678
83. Severns JC, McMillin DR (1990) Temperature and anation studies of the Type 2 site in Rhus vernicifera laccase. Biochemistry 29:8592–8597
84. Reinhammar B (1972) Oxidation-reduction potentials of the electron acceptors in laccases and stellacyanin. Biochim Biophys Acta 275:245–259
85. Fee JA, Malkin R, Malmstrom BG, Vänngard T (1969) Anaerobic oxidation-reduction titrations of fungal laccase : evidence for several high potential electron-accepting sites. J Biol Chem 244:4200–4207
86. Fee JA, Malmström BG, Vanngard T (1969) the reduction of fungal laccase at high pH. Biochim Biophys Acta 197:136–142
87. Farver O, Pecht I (2011) Electron transfer in blue copper proteins. Coord Chem Rev 255:757–773. doi:10.1016/j.ccr.2010.08.005
88. Cole JL, Ballou DP, Solomon EI (1991) Spectroscopic characterization of the peroxide intermediate in the reduction of dioxygen catalyzed by the multicopper oxidases. J Am Chem Soc 113:8544–8546
89. Palmer AE, Quintanar L, Severance S et al (2002) Spectroscopic characterization and O2 reactivity of the trinuclear Cu cluster of mutants of the multicopper oxidase Fet3p. Biochemistry 41:6438–6448
90. Shin W, Sundaram UM, Cole JL et al (1996) Chemical and spectroscopic definition of the peroxide-level intermediate in the multicopper oxidases : relevance to the catalytic mechanism of dioxygen reduction to water. J Am Chem Soc 118:3202–3215
91. Metz M, Solomon EI (2001) dioxygen binding to deoxyhemocyanin: electronic structure and mechanism of the spin-forbidden two-electron reduction of O_2. J Am Chem Soc 123:4938–4950
92. Spira-solomon DJ, Solomon EI (1987) Chemical and spectroscopic studies of the coupled binuclear copper site in Type 2 depleted Rhus laccase: comparison to the hemocyanins and tyrosinase. J Am Chem Soc 109:6421–6432
93. Yoon J, Fujii S, Solomon EI (2009) Geometric and electronic structure differences between the type 3 copper sites of the multicopper oxidases and hemocyanin/tyrosinase. Proc Natl Acad Sci USA 106:6585–6590
94. Yoon J, Solomon EI (2007) Electronic structure of the peroxy intermediate and its correlation to the native intermediate in the multicopper oxidases : insights into the reductive cleavage of the O–O bond. J Am Chem Soc 129:13127–13136
95. Palmer AE, Lee SK, Solomon EI (2001) Decay of the peroxide intermediate in laccase: reductive cleavage of the O–O bond. J Am Chem Soc 123:6591–6599
96. Chen Z, Durao P, Silva CS et al (2010) The role of Glu498 in the dioxygen reactivity of CotA-laccase from Bacillus subtilis. Dalt Trans 39:2875–2882. doi:10.1039/b922734b
97. Silva CS, Damas JM, Chen Z et al (2012) The role of Asp116 in the reductive cleavage of dioxygen to water in CotA laccase: assistance during the proton-transfer mechanism. Acta Crystallogr D Biol Crystallogr 68:186–193. doi:10.1107/S0907444911054503
98. Bukh C, Lund M, Bjerrum MJ (2006) Kinetic studies on the reaction between Trametes villosa laccase and dioxygen. J Inorg Biochem 100:1547–1557. doi:10.1016/j.jinorgbio.2006.05.007

99. Aasa R, Brändén R, Deinum J et al (1976) A paramagnetic intermediate in the reduction of oxygen by reduced laccase. FEBS Lett 61:115–119
100. Lee S-K, George SD, Antholine WE et al (2002) Nature of the intermediate formed in the reduction of O_2 to H_2O at the trinuclear copper cluster active site in native laccase. J Am Chem Soc 124:6180–6193
101. Yoon J, Solomon EI (2005) Ground-state electronic and magnetic properties of a mu3-oxo-bridged trinuclear Cu(II) complex: correlation to the native intermediate of the multicopper oxidases. Inorg Chem 44:8076–8086. doi:10.1021/ic0507870
102. Yoon J, Solomon EI (2007) Electronic structures of exchange coupled trigonal trimeric Cu(II) complexes: spin frustration, antisymmetric exchange, pseudo-A terms, and their relation to O_2 activation in the multicopper oxidases. Coord Chem Rev 251:379–400. doi:10.1016/j.ccr.2006.04.012
103. Yoon J, Liboiron BD, Sarangi R et al (2007) The two oxidized forms of the trinuclear Cu cluster in the multicopper oxidases and mechanism for the decay of the native intermediate. Proc Natl Acad Sci USA 104:13609–13614. doi:10.1073/pnas.0705137104
104. Solomon EI, Augustine AJ, Yoon J (2008) O_2 reduction to H_2O by the multicopper oxidases. Dalton Trans 9226:3921–3932. doi:10.1039/b800799c
105. Branden R, Deinum J (1978) The effect of pH on the oxygen intermediate and the dioxygen reducing site in blue oxidases. Biochim Biophys Acta 524:297–304
106. Branden R, Deinum J, Coleman M (1978) A mass spectrometric investigation of the reaction between 18-O_2 and reduced tree laccase. FEBS Lett 89:180–182
107. Clark PA, Solomon EI (1992) Magnetic circular dichroism spectroscopic definition of the intermediate produced in the reduction of dioxygen to water by native laccase. J Am Chem Soc 114:1108–1110
108. Kataoka K, Sugiyama R, Inoue M et al (2009) Four-electron Reduction of dioxygen by a multicopper oxidase, CueO, and roles of Asp112 and Glu506 located adjacent to the trinuclear copper center. J Biol Chem 284:14405–14413. doi:10.1074/jbc.M808468200
109. Kataoka K, Kitagawa R, Inoue M et al (2005) Point mutations at the type I Cu ligands, Cys457 and Met467, and at the putative proton donor, Asp105, in Myrothecium verrucaria bilirubin oxidase and reactions with dioxygen. Biochemistry 44:7004–7012. doi:10.1021/bi0476836
110. Machonkin TE, Solomon EI (2000) The thermodynamics, kinetics, and molecular mechanism of intramolecular electron transfer in human ceruloplasmin. J Am Chem Soc 122:12547–12560
111. Morishita H, Kurita D, Kataoka K, Sakurai T (2014) Study on dioxygen reduction by mutational modifications of the hydrogen bond network leading from bulk water to the trinuclear copper center in bilirubin oxidase. Biochem Biophys Res Commun 450:767–772. doi:10.1016/j.bbrc.2014.06.052